Accurate K_d *via* Transient Incomplete Separation

Nicolas Sisavath[1], Jean Luc Rukundo[1], J.C. Yves Le Blanc[2], Victor A. Galievsky[1], Jiayin Bao[1], Sven Kochmann[1], Alexander S. Stasheuski[1], and Sergey N. Krylov[1*]

Current methods for finding the equilibrium dissociation constant, K_d, of protein-small molecule complexes have inherent sources of inaccuracy. We introduce "Accurate K_d *via* Transient Incomplete Separation" (AKTIS), an approach that is free of known sources of inaccuracy. Conceptually, in AKTIS, a short plug of the pre-equilibrated protein-small molecule mixture is pressure-propagated in a capillary, causing transient incomplete separation of the complex from the unbound small molecule. A superposition of signals from these two components is measured near the capillary exit as a function of time, for different concentrations of the protein and a constant concentration of the small molecule. Finally, a classical binding isotherm – fraction of unbound small molecule *vs* protein concentration – is built and used to find accurate K_d value. Here we prove AKTIS validity theoretically and by computer simulation, present a fluidic system satisfying AKTIS requirements, and demonstrate practical application of AKTIS to finding K_d of protein-small molecule complexes.

Reversible binding of proteins (P) to small-molecule ligands (L) plays an important role in regulation of cellular processes[1]. In addition, most therapeutic targets are proteins[2], and drugs are developed to form stable PL complexes with them:

$$P+L \rightleftharpoons PL \quad (1)$$

Complex stability is characterized by the equilibrium dissociation constant K_d which is defined as:

$$K_d = \frac{[L]_{eq}[P]_{eq}}{[PL]_{eq}} \quad (2)$$

where $[P]_{eq}$, $[L]_{eq}$, and $[PL]_{eq}$ are equilibrium concentrations of P, L, and PL, respectively. Finding accurate K_d values of PL is pivotal for creating adequate models in systems biology and correctly ranking pharmaceutical hits in early stages of drug development[3].

All available methods for finding K_d of PL have inherent (instrument-independent) sources of inaccuracy. For example, fluorescence spectroscopy (*e.g.* fluorescence anisotropy and fluorescence correlation spectroscopy) and thermophoresis require labeling L with a fluorophore[4]. Attaching a fluorescent label to a small molecule is virtually impossible without affecting its binding[5] and, thus, the accuracy of K_d measurements. Sensor-based techniques, *e.g.* surface plasmon resonance (SPR) and biolayer interferometry (BLI), require the immobilization of either L or P onto a sensor surface[6]. Attaching a molecule to a surface affects binding[7,8] and, thus, accuracy of K_d measurements. Isothermal titration calorimetry (ITC) does not require labeling or immobilization but has another source of inaccuracy: the heat of side reactions, such as binding of L to high-concentration impurities in P, binding of P to P, and solvation of protons released upon L's binding to P[9]. An inherent source of inaccuracy in K_d determined by direct mass-spectrometry (MS) is dissociation of PL during its transfer from the liquid or solid phase to the gas phase and during the ionization[10]. Accuracy of K_d determination with Size-Exclusion Chromatography (SEC) is affected by inevitable adsorption of L, P, and/or PL onto the stationary phase of a SEC column[11]. Finally, finding K_d *via* Taylor Dispersion Assay (TDA) in a capillary requires fast re-equilibration[12–14] and, therefore, becomes inaccurate for stable PL, which re-equilibrate slowly.

As a result of inherent inaccuracies, K_d values determined by different methods for the same PL may deviate by as much as orders of magnitude. Wätzig *et al.* stated in a recent review[15]: "*Binding constants from different laboratories showed an average deviation of approximately 0.5 log units, which translates to a factor of about 3 by which the measurements differ. Surprisingly, this is just the average. The cut-off value not to keep two values in one data set was 2.5 log units which corresponds to a factor of more than 300 by which the measurements differ!*" Such large inaccuracies in K_d values can obviously lead to misinterpretation of experimental results, mistaken conclusions, and misconceptions. This problem motivated our search for an approach for finding K_d of PL that is free of inherent sources of inaccuracy.

Here, we propose "Accurate K_d *via* Transient Incomplete Separation" (AKTIS), an approach for determination of K_d of PL, for which we do not know inherent sources of inaccuracy. Conceptually, a short plug of the pre-equilibrated mixture of P and L is propagated in a capillary by pressure under laminar-flow conditions. Differential transverse diffusion of PL and L in the laminar flow leads to their very fast transient incomplete separation (TIS) in the longitudinal direction. A cumulative signal from protein-bound and protein-unbound L is integrated through the stream cross-section near the capillary exit for different initial concentrations of P and a constant initial concentration of L in the mixture. The signal-*vs*-time dependence is used to calculate a fraction of unbound L for every initial protein concentration. A classical binding isotherm, which is the dependence of the fraction of unbound L on the initial concentration of P, is built. Finally, a value of K_d is found by fitting a theoretical binding isotherm into the experimental one with K_d being a single fitting parameter.

In this proof-of-principle work, we present the theory underlying AKTIS. We conduct computer simulation of the processes involved in AKTIS to demonstrate that AKTIS can accurately recover K_d. We construct an experimental setup that can support AKTIS both with fluorescence and MS detection. Finally, we experimentally demonstrate determination of K_d by AKTIS for two protein small-molecule complexes: bovine serum albumin (BSA)-fluorescein and alpha-1-acid glycoprotein (AGP)-alprenolol. Our results agreed with the consensus data found in the literature. The largest variation in K_d obtained for our measurements on different days with a single detection mode was two folds. Further, the K_d value obtained with fluorescence and MS detection differed by a factor of two. We associate the latter difference with different efficiencies of signal integration through the flow stream cross-section in these two modes of detection. Most of future development of AKTIS should be of

[1]Department of Chemistry and Centre for Research on Biomolecular Interactions, York University, Toronto, Ontario M3J 1P3, Canada.
[2]SCIEX, Concord, Ontario L4K 4V8, Canada. Correspondence should be addressed to S. N. K. (skrylov@yorku.ca)

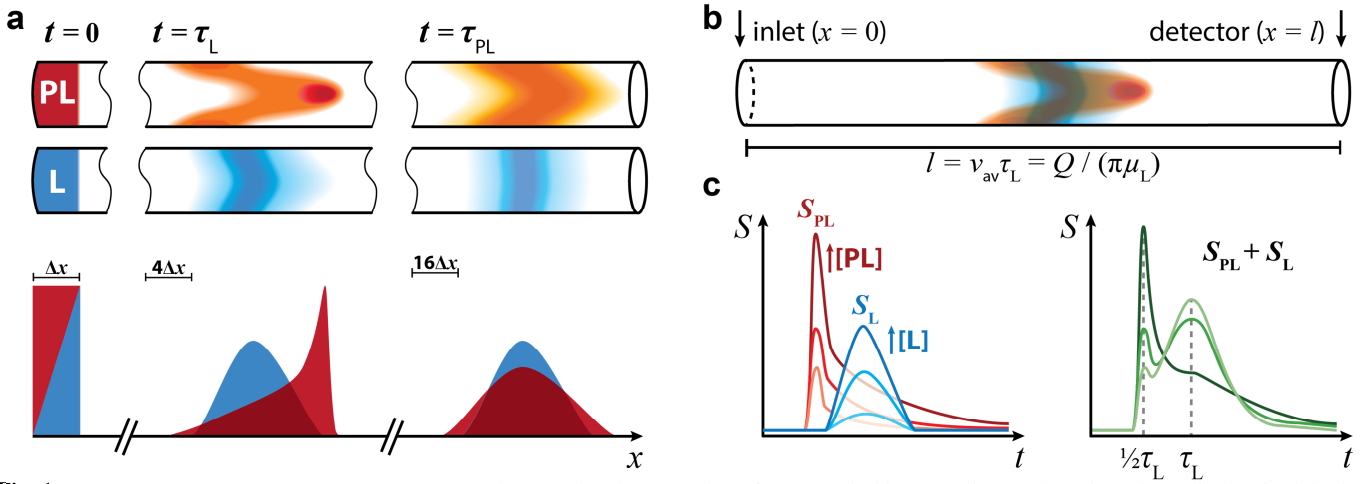

Fig. 1 | Concept of TIS of L (blue) and PL (red). a, TIS in space domain. Top: plugs of L and PL inside the capillary at three times: immediately after injection ($t = 0$), after propagation during a characteristic diffusion time of L ($t = \tau_L$), and after propagation during a characteristic diffusion time of PL ($t = \tau_{PL}$). Bottom: spatial profiles of average cross-sectional concentrations of L and PL at time $t = 0$, $t = \tau_L$, and $t = \tau_{PL}$; Δx refers to the initial plug length at $t = 0$. **b**, Detector positioned at distance $l = v_{av}\tau_L = Q/(\pi\mu_L) >> \Delta x$, were v_{av} is average flow velocity, Q is volumetric TIS flow rate and μ_L is diffusion coefficient of L. **c**, TIS in time domain. Left: individual separagrams of L and PL at their increasing concentrations. Right: example of separagrams for three different values of R.

engineering nature and should aim at optimally coupling the AKTIS fluidic system with different detectors.

Results

General procedure for determination of K_d. In general, finding K_d requires determination of a fraction R of unbound L in the equilibrium mixture (EM) of L and P with the initial concentrations $[L]_0$ and $[P]_0$:

$$R = \frac{[L]_{eq}}{[L]_0} \tag{3}$$

Finding R, in turn, requires a signal S that must be a superposition of signals from L and PL:

$$S = S_L \times R + S_{PL} \times (1 - R), \qquad S_L \neq S_{PL} \tag{4}$$

where S_L and S_{PL} are the signals of pure L ($[L] = [L]_0$, $[PL] = 0$) and pure PL ($[L] = 0$, $[PL] = [L]_0$), respectively; S_L and S_{PL} can be found in experiments with $[P]_0 = 0$ and $[P]_0 >> K_d$, respectively. The signal from pure P must be negligible with respect to S even for $[P]_0 >> K_d$.

From equation (4), R can be experimentally determined *via* measuring three signals S_L, S_{PL}, and S:

$$R_{exp} = (S - S_{PL}) / (S_L - S_{PL}) \tag{5}$$

R can be expressed theoretically as a function of K_d, $[P]_0$, and $[L]_0$[16]:

$$R_{theor} = -\frac{K_d + [P]_0 - [L]_0}{2[L]_0} + \sqrt{\left(\frac{K_d + [P]_0 - [L]_0}{2[L]_0}\right)^2 + \frac{K_d}{[L]_0}} \tag{6}$$

A standard way of finding K_d is to determine R_{exp} for a wide range of $[P]_0$ at a constant $[L]_0$ and to plot a binding isotherm: R_{exp} *vs* $[P]_0$. Finally, this binding isotherm is fitted with equation (6) using K_d as a fitting parameter[16].

TIS of L from PL. We hypothesized that a method for determination of accurate K_d could be built upon a deterministic phenomenon of TIS of solutes with different diffusion coefficients in a laminar pipe flow. TIS is a known phenomenon, which could be predicted as early as in 1910 upon the results of Griffins' experiments with pressure-driven propagation of a fluorescein plug in a narrow tube[17]. Further, TIS could be accurately modeled as early as in 1953 with Taylor's convection-diffusion equations for a diffusive solute in a laminar pipe flow[18]. Finally, the deterministic phenomenon of TIS has been computer-simulated and experimentally studied in multiple works spanning over four decades[19-22]. These studies provided important conceptual pillars and technical details for our work.

TIS of species with largely different sizes, *e.g.* L and PL in our case, occurs always when a plug of their mixture is propagated within a laminar pipe flow in a capillary, which is much longer than the plug (Fig. 1a). Laminar pipe flow is established by a pressure difference between the capillary ends and has a characteristic parabolic profile of flow velocity[23]. The velocity is zero at the capillary walls and reaches its maximum in the capillary center. TIS of L from PL in the longitudinal direction is possible due to the difference in rates of transverse diffusion between small-size L and large-size PL. PL that is near the capillary center will diffuse to the capillary wall slower than L and, thus, will be displaced longitudinally by the flow more than L. PL located near the capillary wall will diffuse to the capillary center slower than L and will be displaced longitudinally by the flow less than L. As a result, during a short transitional stage, a bulk of PL moves faster than a bulk of L, while a tail of PL moves slower than that of L. The separation is incomplete, *i.e.* the concentration profiles of L and PL do overlap, even during the transitional stage. The separation gradually dissipates, *i.e.* the concentration profiles of L and PL become symmetrical around the same symmetry axis, after the transitional stage.

Tracking TIS is practical with a flow system in which the inlet-to-detector distance l is linked with the average flow velocity, v_{av}, characteristic diffusion time of L, τ_L, the volumetric TIS flow rate Q, and diffusion coefficient of L, μ_L, as (Fig. 1b)[23]:

$$l = v_{av}\tau_L = Q/(\pi\mu_L) \tag{7}$$

where v_{av} relates to Q and the inner capillary radius a as:

$$v_{av} = Q/(\pi a^2) \tag{8}$$

The characteristic time of diffusion from the capillary centre to the capillary wall is:

$$\tau = a^2/\mu \tag{9}$$

If TIS is tracked with a system depicted in Fig. 1b, concentration profiles of L and PL will be separated in the time domain as shown in Fig. 1c, left. Further, if a signal can be measured for each of L and PL at the capillary exit and is proportional to the average cross-sectional concentration of each of them, $S_L \propto [L]$ and $S_{PL} \propto [PL]$, then, the cumulative signal S satisfies equation (4) and can, thus, be used to determine R_{exp} with equation (5). This conclusion proves fundamental suitability of TIS for finding K_d of PL.

Examples of the cumulative signal, measured at different values of R, are illustrated in Fig. 1c, right. Traces showing the dependence of the cumulative signal on time, $S(t)$, will be called "separagrams". The choice of a time for measuring S should be governed by minimizing error in R_{exp}. A simple rule is to maximize the value of $(S_L - S_{PL})$ in the denominator of equation (5). Time corresponding to the second peak in the separagram, which is just under τ_L, is a good generic choice. The shortest time for measuring S is near $\frac{1}{2}\tau_L$ (Fig. 1c, right), and according to equation (9) it is mere 0.1 s for L of a size of small-molecule drug ($\mu_L \approx 500$ μm^2/s)[24] and for a capillary radius of $a \approx 10$ μm (such a capillary is commercially available).

We showed above that TIS is theoretically suitable for measuring R_{exp} and, thus, for finding K_d of PL. Unlike both SPR and BLI, TIS does not require immobilization of P or PL. Unlike direct MS, TIS does not require preserving intact PL for detection. Unlike SEC, TIS does not require a stationary phase for separation. Unlike TDA, TIS is equally applicable to weak and stable complexes. Unlike both SEC and TDA, TIS is so fast that adsorption of P, PL, and L onto the wall will typically be negligible. Unlike ITC, TIS is immune to side reactions. Evidently, TIS is free of known sources of inaccuracy present in SPR, BLI, direct MS, SEC, TDA and ITC. Accordingly, we coin a name of "Accurate K_d *via* TIS" (AKTIS) for our approach which (*i*) utilizes TIS to measure R_{exp} as a function of $[P]_0$ resulting in a binding isotherm, and (*ii*) uses the fitting of this binding isotherm with equation (6) to find K_d.

In addition to being free of known sources of inaccuracy, AKTIS is not restricted to a single mode of detection; any detector that can measure a cumulative cross-sectional average signal from L and PL satisfying equation (4) is suitable provided that it has a sufficiently high signal readout speed and a concentration limit of quantitation below K_d values of the studied complexes. A unique advantage of AKTIS is that TIS is based on processes, which are deterministic in nature. These processes can be accurately described by a system of equations for convection-diffusion and reversible binding reaction without any empirical coefficients. As a result, AKTIS separagrams can be accurately computer-simulated and performance of AKTIS can be fully studied *in-silico* before any experimental proof-of-principle is attempted.

AKTIS using a computer-simulated separagrams. TIS is based on three key processes: 1) longitudinal advection of L, P, and PL in a laminar pipe flow, 2) their transverse diffusion, and 3) reversible binding of L and P. Longitudinal diffusion can be neglected[25]. We created a virtual AKTIS setup in COMSOL Multiphysics software and used this virtual setup to simulate separagrams under conditions similar to realistic ones in an envisioned proof-of-principle experiment (see Materials and Methods and Supplementary Note 1).

The virtual setup was used to simulate an experiment in which: 1) EM (equilibrium mixture of L and P) was prepared outside the capillary in a solvent with properties of water, 2) a short plug of EM (sample plug) was injected by pressure-driven flow with a small flow rate of $0.1Q$ into the capillary pre-filled with water, 3) a plug of water was injected into the capillary with a small flow rate of $0.1Q$ to slowly displace the sample plug from the capillary inlet, 4) water was continuously pumped into the capillary at a high flow rate of Q to induce TIS of L from PL and P, 5) concentrations of L, PL, and P

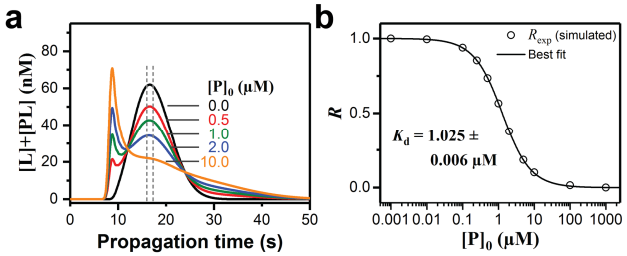

Fig. 2 | Determination of K_d by AKTIS using computer-simulated separagrams. a, Representative separagrams for $[L]_0 = 0.5$ μM, $[P]_0$ ranging from 0 to $10K_d$, $k_{off} = 10^{-3}$ s^{-1}, $k_{on} = 10^3$ M^{-1} s^{-1} ($K_d = k_{off}/k_{on} = 1$ μM), $\mu_L = 500$ μm^2/s, $\mu_P = \mu_{PL} = 50$ μm^2/s, internal capillary radius $a = 100$ μm, inlet-to-detector distance $l = 1$ cm, sample-plug injection flow rate = 0.1 μL/min, sample-plug injection time = 12 s, sample-plug displacement flow rate = 0.1 μL/min, sample-plug displacement time = 12 s, TIS flow rate $Q = 1$ μL/min. The ordinate shows a sum of cross-sectional averages of [L] and [PL] in the detection window. This cumulative concentration, taken as average between the times shown with the dashed lines, was used as a signal in equation (10) to calculate R_{exp}. **b**, A binding isotherm R_{exp} *vs* $[P]_0$ (open circles), the best fit of the binding isotherm with equation (6) (solid line), and the K_d value corresponding to the best fit.

(determined as integrals of quantities of L, PL, and P through a cylindrical finite-length capillary cross-section divided by the volume of this cylinder) were recorded at the capillary end as functions of time, and 6) a sum of concentrations of L and PL was used to construct a separagram. Here and further we assume that P and PL have identical diffusion coefficients due to only a small difference in their hydrodynamic sizes.

The simulation parameters and results are readily scalable to any feasible l and Q, as long as their ratio satisfies $l/Q \approx 1/(\pi\mu_L)$ (obtained from equation (7))[26,27]. Thus, an experimental setup with, *e.g.* $l = 50$ cm, $Q = 50$ μL/min, and sample-injection flow rate of 5 μL/min could be simulated with 50 times lower values (1 cm, 1 μL/min, and 0.1 μL/min) to reduce computational time by approximately a factor of 50 (from hours to minutes). The remaining parameters (diffusion coefficients, rate constants, concentrations, and capillary radius) were set at realistic values.

Representative separagrams simulated in the virtual experiment are shown in Fig. 2a. Signals required for determination of R_{exp} were obtained by averaging points within a time-window near t_L (= 20 s). The middle of the window corresponded exactly to the maximum of the second peak (*e.g.* 16.63 s in Fig. 2a). The first point and last point of the window corresponded exactly to 0.96 and 1.04 of the maximum of the second peak (Materials and Methods), respectively (*e.g.* 15.97 s and 17.30 s in Fig. 2a). Further, the fraction R_{exp} of unbound L at a given intermediate value of $[P]_0$ was determined with a slightly modified equation (5):

$$R_{exp} = \frac{S - S_{PL}}{S_L - S_{PL}} \approx \frac{S_{[P]_0} - S_{[P]_0 \gg K_d}}{S_{[P]_0 \ll K_d} - S_{[P]_0 \gg K_d}} \qquad (10)$$

where $S_{[P]_0}$ is a signal at the intermediate value of $[P]_0$. Here and in the following, we approximate S_{PL} with $S_{[P]_0 \gg Kd}$ and S_L with $S_{[P]_0 \ll Kd}$. The main reason for such approximation is that strictly speaking S_{PL} corresponds to $[PL] = [L]_0$ which cannot be achieved in a real experiment since it requires $[P] \to \infty$. Therefore S_{PL} is approximated with $S_{[P]_0 \gg Kd}$, and, symmetrically, S_L is approximated with $S_{[P]_0 \ll Kd}$.

The values of R_{exp}, determined from the simulated separagrams in Fig. 2a with equation (10), were used to build a binding isotherm

shown in Fig. 2b. Non-linear regression was used to fit the isotherm with R_{theor} represented by equation (6) with K_d being a single fitting parameter. The best fit is shown as a solid line in Fig. 2b. The K_d value that corresponded to the best fit differed from the one used in simulations by only 3%. The deviation from the ideal value was expected. Our virtual experiment included a number of non-idealities of a real experiment. For example, the initial plug after injection by finite pressure had finite length and a non-cylindrical shape. The limited number of points in the binding isotherm (like in a real experiment) also contributes to the observed deviation.

The choice of $l/Q = 1/(\pi\mu_L)$ is governed by the value of μ_L, and, thus, is a subject to errors associated with uncertainties in μ_L. The value of μ_L may range from about 300 to 1500 $\mu m^2/s$ for organic molecules with MW < 1000 Da[28]. In practice, the value of μ_L is not known precisely. To study robustness of AKTIS to uncertainties in μ_L we simulated separagrams with l/Q ranging from $1/(3\pi\mu_L)$ to $3/(\pi\mu_L)$, which is in the range of expected variations for $\mu_L = 500$ $\mu m^2/s$ chosen as the value for the first set of simulations (see Fig. 2). The resulting separagrams are shown in Supplementary Fig. 1. They are qualitatively similar to those obtained for $l/Q = 1/(\pi\mu_L)$. The values of R_{exp} were calculated for times corresponding to the maximum of the second peak (as in Fig. 2a) and K_d values were found not to deviate more than 5% from the value used in simulations, proving that AKTIS is robust with regards to the choice of l/Q, and suggesting that a single value of l/Q can be used to study L greatly varying in size. Thus, our study of AKTIS applied to simulated separagrams showed that AKTIS is accurate and robust.

Quenching and masking effects in signal detection. In our above-described *in-silico* study of AKTIS, we used a direct link between the signal and a cumulative concentration of L and PL: $S = [L] + [PL]$. In reality, the signals from L and PL depend on the nature of both P and L as well as the mode of detection. P can influence the signal from L by binding L (we'll call this influence "quenching") and by being in the detector at the time of registration (we'll call this influence "masking").

If optical (*e.g.* fluorescence) detection is used, static quenching with a constant quenching coefficient is likely to be present. On the other hand, masking (*i.e.* dynamic quenching) in optical detection is unlikely. As a result, the signal in optical detection is multiplied with a constant quenching coefficient. Therefore, the signal will satisfy the requirement of signal superposition expressed by equation (4). Thus, while static quenching will affect separagrams, its presence will not affect the K_d value determined with the AKTIS procedure illustrated in Fig. 2.

If MS is used for detection of L, conditions should be created to dissociate PL during ionization to exclude the need for detecting the intact PL. The dissociation of PL will automatically exclude signal quenching. However, the presence of unbound P can affect ionization of unbound L and, in turn, signal from L[10,29], causing its masking (either increase or decrease in the signal). To "unmask" the signal, an operator $\hat{O}$, which describes a mathematical compensation procedure, should be applied to the raw MS signal $S_{raw}(t)$:

$$S(t) = \hat{O}S_{raw}(t) \qquad (11)$$

Subsequently, this "unmasked" signal can be used for K_d determination using the standard AKTIS protocol.

A simple masking-compensation procedure can be built upon two facts. First, P and PL have similar separagrams; these separagrams can be robustly and accurately computer-simulated. Second, the concentration (and amount) of L is constant in experiments with varying $[P]_0$; thus, the areas under the separagrams should be constant. Based on these two facts, we suggest a compensation procedure with two operations: 1) multiplication (operator $\hat{O}_M$) of the measured separagrams by the simulated profile of P and 2) subsequent normalization (operator $\hat{O}_N$) of the separagrams to make the areas (integrals) under them equal to the area (integral) under the experimental separagram of L corresponding to the smallest amounts of protein ($[P]_0 << K_d$):

$$\hat{O} \equiv \hat{O}_N\hat{O}_M, \quad \hat{O}_M = \tilde{S}_P(t), \quad \hat{O}_N = \frac{\int \tilde{S}_P(t)S_{[P]_0<<K_d}(t)dt}{\int \tilde{S}_P(t)S_{raw}(t)dt} \qquad (12)$$

where $\tilde{S}_P$ is the dimensionless simulated separagram of pure P. $\hat{O}_N$ can be greater or smaller than unity, *i.e.* the presence of P can either suppress or enhance ionization of L. Combining equation (11) with equation (12) provides an instruction on how to process the raw signal in order to get the unmasked signal for K_d determination:

$$S(t) = \frac{\int \tilde{S}_P(t)S_{[P]_0<<K_d}(t)dt}{\int \tilde{S}_P(t)S_{raw}(t)dt}\tilde{S}_P(t)S_{raw}(t) \qquad (13)$$

This unmasked signal can be used in equation (10) to find R_{exp} and determine K_d.

The described compensation procedure limits the compensated effect of P on the signal from L to the linear term: masking is proportional to the concentration of P. While higher-order effects are theoretically possible, they are assumed to have lower weights than the linear effect. This compensation procedure automatically becomes null in the absence of masking; therefore, it can be applied by default when MS detection is used for AKTIS.

Fluidic system for AKTIS. Our *in-silico* studies proved that AKTIS can be used for finding accurate K_d of reversible protein-small molecule binding provided that an experimental setup can be built to conduct experiments similar to the simulated ones. In an experimental implementation of AKTIS we attempted to mimic *in-silico* studies in which plugs of identical volumes were injected by a constant low flow rate and TIS was carried out by a constant high flow rate. Our fluidic system is shown schematically in Fig. 3. In this system, the equality of plug volumes is achieved by using a fixed-volume injection loop fed from a sample injection pump. The constancy of flow rates for sample injection and TIS is achieved by using two continuously running pumps under constant back-pressures: the low-pressure pump (LPP) for sample transfer from the injection loop into the separation capillary and high-pressure pump (HPP) for TIS. Constant back-pressures are achieved, in turn, by using a mock fluidic circuit: a mock injection loop and a mock capillary of dimensions identical to those of the main injection loop and the separation capillary.

The operation of the AKTIS fluidic system involved three major stages with a total duration of 86 s. Transitions between these stages were carried out by switching fluidic connections with control valves; the switch time did not exceed 0.1 s. Stage 1 was the loading of the injection loop with the sample during 12 s (Fig. 3a). The sample was slowly pumped through the loop by the sample pump. The volume of the pumped sample was equal to three volumes of the loop; the excess of the sample was collected into the waste reservoir. During this stage, the HPP was pumping the buffer through the separation capillary and cleaning the capillary, and the LPP was pumping the buffer through the mock fluidic circuit. Stage 2 was sample-plug transfer into the separation capillary during 24 s (Fig. 3b). The LPP was pumping the buffer into the injection loop filled with the sample and slowly transferring the sample from the injection loop into the separation capillary. It is known that a velocity profile of laminar flow is distorted at the capillary entrance open to a reservoir of a different diameter[30]; therefore, the sample plug was injected into the capillary so that its back was at a distance from the capillary inlet much greater than the capillary diameter (3.2 *vs* 0.02 cm in our case). During this stage the sample pump was idle

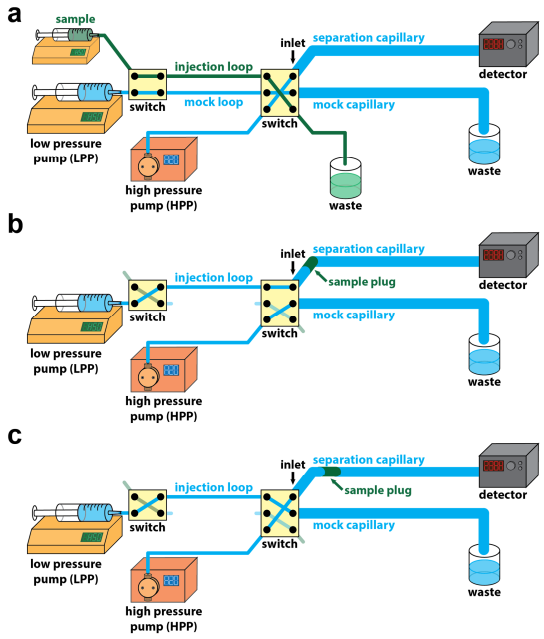

Fig. 3 | Schematic of AKTIS fluidic system. a, Sample loading into the injection loop required for precisely dosing sample volume; LPP is pumping the buffer through a mock loop into a mock capillary, and HPP is pumping the buffer through the separation capillary. **b,** Transfer of the sample plug from the injection loop into the separation capillary by LPP using a low flow rate to maintain the near-cylindrical plug shape; the sample pump is idle (not shown), and HPP is pumping the buffer through the mock capillary. **c,** Propagation of the sample plug by HPP using a high flow rate and causing TIS of PL from L registered with a detector; the sample pump is idle (not shown), and LPP is pumping the buffer through the injection loop and the mock capillary. The mock loop and mock capillary mimic the injection loop and separation capillary, respectively, and allow LPP and HPP to run continuously under constant back-pressures. For details on instrumentation see Materials and Methods and Supplementary Fig. 2.

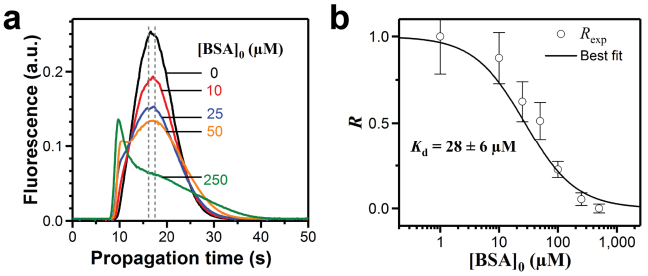

Fig. 4 | Determination of K_d by AKTIS with fluorescence detection. a, Representative separagrams for BSA-fluorescein complex from a set of separagrams obtained for $[\text{fluorescein}]_0 = 0.2$ μM and $[\text{BSA}]_0$ ranging from 0 to 0.5 mM. The vertical dashed lines show the time window at which an averaged signal was taken to calculate R_{exp} with equation (10). Experimental conditions were: internal capillary radius $a =$ 100 μm, inlet-to-detector distance $l =$ 50 cm, injection loop's internal radius = 37.5 μm, injection loop's length = 22.7 cm (injection loop's volume = 1 μL), sample loading into the injection loop at a flow rate of 15 μL/min during 12 s, sample-plug transfer to the separation capillary at a flow rate of 5 μL/min during 24 s (plug length = 3.2 cm, plug end distance from the capillary inlet = 3.2 cm), TIS flow rate $Q = 50$ μL/min, 30 mM ammonium acetate buffer pH 7.5. **b**, A binding isotherm R_{exp} *vs* $[\text{P}]_0$ (open circles, $n \geq 7$) and the best fit of the binding isotherm with equation (6) (solid line). The uncertainty of R was obtained by error propagation using equation (10) (Supplementary Note 2).

and the HPP was pumping the buffer through the mock capillary. Stage 3 was sample-plug propagation by HPP and, thus, TIS of PL from L duing 50 s. During this stage the sample pump was filling the tube connecting the sample syringe with the injection loop, and the LPP was pumping the buffer through the injection loop and the mock capillary. The beginning of stage 3 was used as a starting point for the corresponding separagram. More details on the AKTIS fluidic system can be found in Materials and Methods and Supplementary Fig. 2.

AKTIS with fluorescence detection. The first set of AKTIS experiments was performed with BSA (P) and fluorescein (L) using a fluorescence detector. The obtained separagrams had typical TIS shapes with two peaks. The results revealed high repeatability (Supplementary Fig. 3). Equation (10) was applied to experimental data from Fig. 4a, and a binding isotherm was constructed (Fig. 4b). Non-linear regression of the isotherm with equation (6) gave $K_d = 28 \pm 6$ μM. When reproduced on other days, the results varied between 12 ± 3 μM and 26 ± 3 μM (Supplementary Fig. 4).

AKTIS with MS detection. We coupled our AKTIS setup with an MS detector. To facilitate dissociation of PL during ionization, we utilized an Atmospheric Pressure Chemical Ionization source (see Materials and Methods). AKTIS-MS was used to determine K_d for two protein-ligand complexes: BSA-fluorescein and AGP-alprenolol (Fig. 5) The AKTIS-MS measurements reveled opposite masking effects for these two binding pairs: MS signal from fluorescein decreased with increasing $[\text{BSA}]_0$ (Fig. 5a, left), while MS signal from alprenolol increased with increasing $[\text{AGP}]_0$ (Fig. 5b, left). Separagrams were highly repeatable (Supplementary Figs. 5,6). We applied our two-step signal-unmasking procedure to both sets of separagrams and obtained unmasked separagrams with characteristic TIS features (Figs. 5a,b, middle). Equation (10) was then used to build binding isotherms (Figs. 5a,b, right). Finally, equation (6) was used to fit the isotherms and find $K_d = 31 \pm 4$ μM for the BSA-fluorescein complex and $K_d = 1.4 \pm 0.2$ μM for the AGP-alprenolol complex. The largest deviation from these values obtained on different days did not exceed two folds: $K_d = 44 \pm 4$ μM for BSA-fluorescein and $K_d = 2.7 \pm 0.6$ μM for AGP-alprenolol (Supplementary Figs. 7,8). The K_d value for BSA-fluorescein obtained with AKTIS-MS is approximately two times higher than the value obtained by AKTIS with fluorescence detection. Our K_d values agree with the literature values for both BSA-fluorescein (10–70 μM)[31–33] and AGP-alprenolol (2–35 μM)[34–37] complexes.

Discussion

In this proof-of-principle work, we introduce AKTIS as a generic approach for measuring accurate K_d of protein-small molecule complexes. While relying on separation, AKTIS does not require any form of stationary phase and does not impose any requirements on the protein and the small molecule except for the requirement of their different sizes. AKTIS does not require immobilization of the protein or small molecule. TIS can be achieved even in a sub-second time scale, making AKTIS applicable to very unstable protein-ligand complexes. On the other hand, AKTIS is perfectly applicable to stable complexes. The short time of TIS should prevent inaccuracies associated with adsorption of the protein-ligand complex or the ligand onto the capillary wall. In the case of severe adsorption that influences the results, the capillary inner wall can be passivated with any kind of chemistry; TIS should not be affected by such capillary

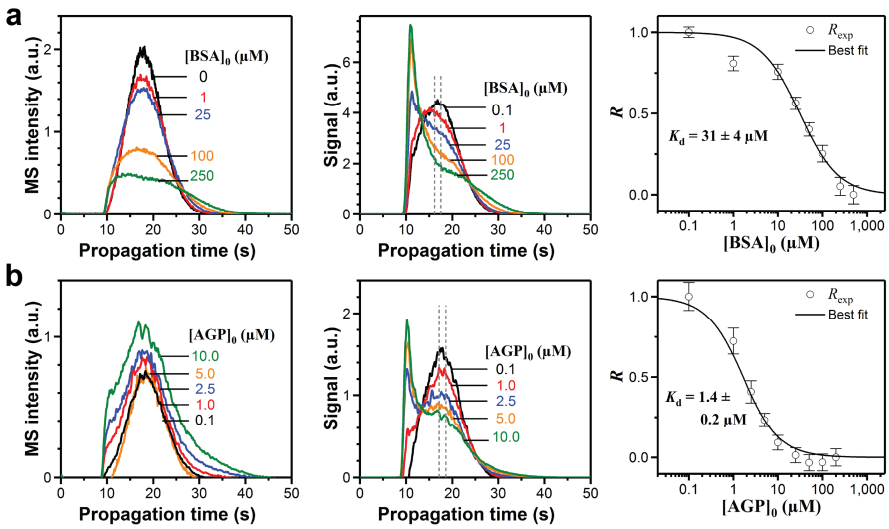

Fig. 5. | **Determination of K_d by AKTIS with MS detection. a**, Determination of K_d for the BSA-fluorescein complex; $[\text{fluorescein}]_0 = 0.2$ μM and $[\text{BSA}]_0$ ranges from 0 to 0.5 mM. MS signal for fluorescein was measured at $m/z = 287$. **b**, Determination of K_d for the AGP-alprenolol complex; $[\text{alprenolol}]_0 = 0.5$ μM and $[\text{AGP}]_0$ ranges from 0 to 0.2 mM. MS signal for alprenolol was measured at $m/z = 250$. Left: representative raw separagrams. Middle: separagrams after application of the signal-unmasking procedure; the vertical dashed lines show the time window at which an averaged signal was taken to calculate R_{exp} with equation (10). Right: binding isotherms R_{exp} *vs* $[\text{P}]_0$ (open circles) and their best fits (solid lines) obtained with equation (6). Conditions for AKTIS were similar to those described in the legend to Fig. 4 except for $l = 100$ cm and $Q = 100$ μL/min (l/Q was the same). The uncertainty of R was obtained by error propagation (Supplementary Note 3).

modification if this modification does not introduce non-uniformity of capillary radius along the capillary.

While being free of instrument-independent sources of inaccuracy, AKTIS is expectedly susceptible to errors associated with instrumentation. For example, potential inability to uniformly integrate the signal through the entire capillary cross-section may lead to systematic errors. Therefore, optimally coupling the AKTIS fluidic system with different detectors will require further efforts of the engineering nature which were not undertaken in this work. The observed two-fold difference in K_d found by AKTIS-fluorescence and AKTIS-MS is most likely associated with the mentioned inaccuracies of signal integration. Instrument-independent errors in K_d can be caused by uncertainty in protein concentration, *e.g.* due to errors in its measurements or due to protein degradation. This uncertainty is likely the reason for day-to-day variations in K_d values observed in our experiments. The uncertainty in active protein concentration can be taken care of by using a more elaborate way of data collection, which includes the variation of both protein concentration and ligand concentration. In this way, both K_d and active protein concentration can be found simultaneously *via* varying both K_d and $[\text{P}]_0$ when fitting equation (6) into a binding isotherm[16].

AKTIS can be combined with any detection method which (*i*) can be coupled with a capillary, (*ii*) uniformly integrates the signal through the capillary cross-section, (*iii*) has sufficiently high signal readout speed, and (*iv*) has a concentration limit of quantitation below K_d values of the studied complexes. A combination of AKTIS with MS appears to be the most suitable one for protein small-molecule complexes as it allows label-free detection of small molecules. If AKTIS proves to be applicable to complexes of proteins of significantly different sizes, it can potentially be used for screening antibodies against small-size protein antigens. This application may justify preparing a fluorescent modification of the antigen and using AKTIS with fluorescence detection for screening antibodies against such an antigen. In general, we foresee that most of future technical development of AKTIS will deal with its coupling with different detection systems and satisfying the four above-listed AKTIS requirement to detection systems.

Materials and Methods

General. All chemicals and buffer components were purchased from Sigma-Aldrich (Oakville, ON, Canada). Fused-silica capillaries were purchased from Molex (Polymicro Technologies, Phoenix, AZ, USA). All measurements were carried out at room temperature (22 ± 2 °C). A single buffer, 30 mM ammonium acetate pH 7.5, was utilized to prepare all solutions. When we refer to the buffer, we mean 30 mM ammonium acetate pH 7.5.

Simulation of separagrams. To simulate separagrams we used COMSOL Multiphysics software, version 5.3, with the "Transport of Diluted Species" module, which incorporates mass transfer equations (the model is available in the Supplementary files). The respective system of differential equations with initial and boundary conditions are shown in Supplementary Note 1. The laminar flow can be obtained if the Reynolds number, $Re \equiv 2Q/(\nu_k \pi a)$, is less than a thousand, where Q is the volumetric flow rate, ν_k is the kinematic viscosity of a liquid, and a is the capillary internal radius. As a result, water ($\nu_k \approx 10^{-6}$ m^2/s) will have laminar flow in narrow capillaries ($a \approx 100$ μm) as long as $Q \leq 1$ mL/min. The simulation parameters were chosen to ensure that the flow is laminar.

The simulation parameters were also chosen in order to have the detection time of the peak of L corresponding to the characteristic diffusion time of L as discussed in the main text (see equation (9)). This condition resulted in the following ratio: $l/Q \approx 1/(\pi\mu_L)$. Considering L with $\mu_L = 500$ μm^2/s, and a capillary with an internal radius $a = 100$ μm, the detection time would be 20 s, which is a reasonable value for the prototype experimental setup. Computational time depends on the dimensions of the simulated capillary. Thus, to reduce this time, the inlet-to-detector distance l can be scaled down while the ratio l/Q is kept constant. $l = 1$ cm and detection window of 0.1 mm were chosen which resulted in the flow rate of $Q \approx 0.9$ μL/min and for simplicity $Q = 1$ μL/min was used. Sample plug injection flow rate should be smaller than TIS flow rate. Thus, sample-plug injection was done with a flow rate of 0.1 μL/min during 12 s resulting in a near-rectangular injection plug

of approximately 0.6 mm in length. Subsequently, a water plug was injected into the capillary with 0.1 µL/min during 12 s to slowly displace the sample-plug from the capillary inlet (plug end distance from the capillary inlet was approximately 0.6 mm). The rest of simulation parameters were as follows: $k_{off} = 10^{-3}$ s^{-1}, $k_{on} = 10^3$ $M^{-1}s^{-1}$ ($K_d = k_{off}/k_{on} = 1$ µM), $\mu_P = \mu_{PL} = 50$ µm^2/s, $[L]_0 = 0.5$ µM, temperature = 293.15 K (used by COMSOL to define physical parameters of water, *e.g.* viscosity and density). $[P]_0$ was varied from 1 nM to 1 mM using 11 different concentrations plus a run at $[P]_0 = 0$. Further, to study robustness of AKTIS to uncertainties in $\mu_L = 500$ µm^2/s we simulated separagrams with l/Q ranging from $1/(3\pi\mu_L)$ to $3/(\pi\mu_L)$ by varying l (Supplementary Fig. 1).

Since the plug shape is symmetric with respect to the capillary longitudinal axis, the capillary was modeled with a 2D axisymmetric shape to further reduce the computation time. The virtual detector was placed at the end of the virtual capillary. The modeled shape of the capillary was divided into a rectangular mesh with a density of 5000 cells (20 × 250, radial and axial mesh) per centimeter. The detection zone for each l (1 cm as well as 1/3 cm, 1/2 cm, 2 cm and 3 cm) was also divided into a rectangular mesh but with 200 cells (20 × 10, radial and axial mesh). The Iterative Generalized Minimal Residual (GMRES) solver was used in COMSOL to approximate concentrations of reactive species in a time-dependent manner over the defined mesh. The output signal was defined as a sum of individually averaged concentrations of L and PL inside the 200-cell detection zone.

AKTIS fluidic setup. A general schematic of the AKTIS fluidic setup is shown in Fig. 3 and a more detailed schematic emphasizing valve operation during the measurement cycle is shown in Supplementary Fig. 2. Custom software written in LabVIEW was utilized to control the valves via a PCI-6035E board (National Instruments, Austin, TX, USA).

Buffer and sample solutions were injected by NE-300 syringe pumps (New Era Pump Systems Inc., Farmingdale, NY, USA) utilizing syringes of 10 mL and 1 mL, respectively (Becton, Dickinson and Company; Mississauga, ON, Canada). While being identical, these pumps had different functions and were named the "sample pump" and the low pressure pump (LPP) for sample loading and sample transfer, respectively. The sample plug was propagated through the separation capillary by a high pressure pump (HPP) from a solvent delivery module of System Gold HPLC 128NM (Beckman Coulter, Fullerton, CA, USA) for fluorescence measurements and by HPP from Nexera SR System HPLC module (Shimadzu Scientific Instruments, MD, USA) for MS measurements. Two dual-position valves (Rheodyne MXP7900-000 from IDEX Health & Science, Oak Harbor, WA, USA) were used to switch flow pathways in the fluidic setup. The sample syringe was connected to Valve 1 with a 30-cm long uncoated fused-silica capillary of 150-µm inner diameter and 360-µm outer diameter (through capillary tubing fittings from IDEX Health & Science); this capillary was pre-filled with the sample before the Sample loading stage (see below). The buffer syringe was connected to the valves using a polyethylene tubing of 1.57-mm inner diameter and 2.08-mm outer diameter (BD Intramedic, purchased from Fisher Scientific, Ottawa, ON, Canada). An uncoated fused-silica capillary of 75-µm inner diameter, 360-µm outer diameter, and 22.7-cm length was utilized as an injection loop with a volume of $V_{loop} = 1$ µL. The injection loop was placed between Valves 1 and 2. An additional mock loop identical to the injection loop was positioned between Valves 1 and 2. An uncoated fused-silica capillary of 200-µm inner diameter and 360-µm outer diameter was used for TIS and is named "separation capillary"; it was connected to Valve 2. The total length of the capillary was 60 cm (inlet-to-detector distance was $l = 50$ cm) for a setup with fluorescence detection and 100 cm (inlet-to-detector distance was $l = 100$ cm) for a setup with MS detection. Two mock capillaries identical to the separation capillary were connected to Valve 2. The mock loop and the mock capillaries were used to allow the continuous operation of LPP and HPP and ensure that they ran under constant back-pressures.

The pumps operated at the following flow rates: the sample pump at 15 µL/min, LPP at 5 µL/min, HPP for fluorescence detection at $Q = 50$ µL/min and HPP for MS detection at $Q = 100$ µL/min (to keep l/Q = const = 1 cm min µL^{-1}). An 86-s-long measurement cycle included 3 stages. Switching between the stages was done by changing positions of the valves during less than 0.1 s. For the very first run and cycle, the sample was pre-filled into the capillary connecting the sample pump and Valve 1 (using its position II) before starting the cycle; in subsequent runs and cycles, this pre-filling was done during the third stage.

The first stage was 12-s-long sample loading into the 1-µL injection loop (Supplementary Fig. 2a). Valves 1 and 2 were in position I. The sample pump moved sample volume equal to $3 \times V_{loop}$ through the injection loop to insure its complete filling. LPP was pumping the buffer through the mock loop and mock capillary. HPP was pumping the buffer through the separation capillary.

The second stage was 24-s-long sample transfer from the injection loop into the separation capillary (Supplementary Fig. 2b). Both valves were in position II. LPP moved the buffer *via* the sample-containing injection loop. The sample was subsequently transferred into the separation capillary. At the end of this stage a sample plug of approximately 3.2 cm in length was 3.2 cm away from the inlet of the separation capillary. HPP was pumping the buffer through the mock capillary. The sample pump was idle.

The third stage was 50-s-long sample propagation through the separation capillary (Supplementary Fig. 2c). Valve 2 was in position I, while Valve 1 stayed in position II. The sample pump was used for pre-filling. HPP pumped the buffer into the separation capillary for TIS of PL from L. LPP was pumping the buffer through the injection loop. In total the injection loop was rinsed with $6 \times V_{loop}$ ($2 \times V_{loop}$ during the second stage and $\approx 4 \times V_{loop}$ during the third stage).

Fluorescence detector. A diode-pumped solid state laser (AixiZ, Houston, TX, USA) was a light source for excitation of fluorescence. The laser beam had a diameter of about 2 mm and a power of 60 mW at 473 nm. Two subsequent neutral filters of 0.4 and 1.0 optical density (NE04B and NE10B, Thorlabs, Newton, NJ, USA) were used to attenuate laser power to ≈ 2 mW. Fluorescence emission was collected by an MPlan 60× objective lens (NA = 0.7 at 90°) with an additional optical bandpass filter of 525 ± 25 nm (Semrock, Rochester, NY, USA). A photocathode of the photomultiplier tube R1477 (Hamamatsu Photonics, Hamamatsu, Japan) was biased at −400 V. A 20 Hz low-pass electronic filter was introduced between the photomultiplier tube and the analog-to-digital signal converter PCI-6035E (National Instruments, Austin, TX, USA), to reduce electronic noise. Fluorescence data collection was controlled with the same custom LabVIEW software that was used to control the valves in the fluidic setup.

Fluorescence-based determination of K_d for the fluorescein-BSA complex. Concentration of fluorescein was 0.2 µM. Concentration of BSA ranged from 0.1 µM to 1 mM. Fluorescein-BSA mixtures were vortexed and incubated at room temperature for ≈ 2 h to establish equilibrium in the reversible binding reaction. After the incubation, the EMs were subjected to AKTIS as described in the "AKTIS fluidic setup" section. To obtain R_{exp} for each BSA

concentration the experiment was repeated at least 5 times. The value of K_d was obtained by fitting R_{exp} *vs* $[P]_0$ with R_{theor} *vs* $[P]_0$ as described in the "Data acquisition and treatment" section.

MS detector. The output of the separation capillary was inserted into the MS ionization source (Turbo V ion source with APCI probe, AB Sciex, Vaughan, ON, Canada). MS detection was done with a QTRAP 6500+ instrument (AB Sciex, Vaughan, ON, Canada). The optimal acceleration and focusing conditions were achieved by using a 60-V declustering potential at 525 ºC and 90-psi gas pressure. The MS analyses were performed in positive mode, and the analyzed small molecules – fluorescein and alprenolol – were detected at *m/z* of 287 and 250, respectively. The *m/z* signals were processed using Analyst QS 2.0 software. MS data collection was controlled with the same custom LabVIEW software and PCI-6035E board that were used to control the valves in the fluidic setup.

Determination of K_d for fluorescein-BSA and alprenolol-AGP complexes by AKTIS with MS detection. The experiments were performed to measure K_d of complexes between BSA (0.1–500 µM) and fluorescein (0.2 µM) as well as between AGP (0.1–500 µM) and alprenolol (0.5 µM). BSA-fluorescein and AGP- alprenolol mixtures were incubated at room temperature for ≈ 2 h to establish equilibrium in the reversible binding reaction. After incubation, the EMs were subjected to AKTIS as described in the "AKTIS fluidic setup" section. Measurements of R_{exp} for each protein concentration were done in triplicates. K_d was obtained by fitting R_{exp} *vs* $[P]_0$ with R_{theor} *vs* $[P]_0$ as described in the "Data acquisition and treatment" section.

Data acquisition and treatment. The experimental data acquisition was triggered at the beginning of the sample-transfer stage (second stage); this mimicked the way of treatment of simulated separagrams. The acquired or simulated data were evaluated using Excel and OriginPro (files are available in the Supplementary). For each experimental signal of the MS data the background taken at the beginning of the recorded separagram ($t < 5$ s) was subtracted; the background of the fluorescence data was already within the limits of signal noise and, hence, was not subtracted. Equation (10) was used to calculate R_{exp}. Signals required for determination of R_{exp} were obtained by averaging points within a time-window near $\tau_L = 20$ s. The middle of the window corresponded exactly to the maximum of the second peak (*e.g.* 16.63 s in Fig. 2a) taken from the separagram of the smallest $[P]_0 \neq 0$. The first point and the last point of the window corresponded exactly to 0.96 and 1.04 of the position of this maximum of the second peak, respectively (*e.g.* 15.97 s and 17.30 s in Fig. 2a). This window width was chosen to increase the signal-to-noise ratio while covering only the tip of the peak; for our data, the window width ranged between 1.2 and 1.5 s. The averaged signal at each concentration of sample was measured/simulated $n \geq 3$ times. The standard deviation (σ) for each R_{exp} was obtained by simple error propagation based on equation (10) (Supplementary Notes 2 and 3). K_d was obtained by fitting the dependence of R_{exp} on $[P]_0$ with equation (6) (see main text). A weighted non-linear fitting was performed using the Levenberg-Marquardt algorithm; each point had a weight of σ^{-2}.

Data and model availability. The COMSOL model as well as the raw data and evaluated data for separagrams and binding isotherms in Figs. 2, 4, and 5 and Supplementary Figs. 1, 3-8 are provided as Supplementary files to the paper.

Acknowledgements
This work was supported by the Natural Sciences and Engineering Research Council of Canada (grant number STPG-P 521331-2018) and Mitacs Canada (grant number IT08656).

Author contributions
N.S. performed the experiments, analyzed the data, developed software, and wrote the manuscript. J.L.R. performed the experiments, analyzed the data, developed software, and wrote the manuscript. J.C.Y.L.B. and J.B. helped with MS experimental design and MS experiments. V.A.G. and A.S.S. helped with fluorescence experiments, developed software, and wrote the manuscript. S.K. analyzed data, designed figures, helped with the mathematical formulation, and wrote the manuscript. S.N.K. conceptualized, conceived, and guided the study, designed experiments, suggested design of the AKTIS instrument, proposed the masking-compensation procedure, interpreted the data and wrote the manuscript. All authors reviewed and approved the manuscript.

Competing interests
The authors declare no competing financial interests.

1. Firestone, A. J. & Chen, J. K. Controlling destiny through chemistry: small-molecule regulators of cell fate. *ACS Chem. Biol.* **5,** 15–34 (2010).
2. Zheng, C. J., Han, L.Y., Yap, C. W., Cao, Z. W. & Chen, Y. Z., Therapeutic targets: progress of their exploration and investigation of their characteristics. *Pharmacol. Rev.* **58,** 259–279 (2006).
3. Cooper, M. A. Optical biosensors in drug discovery. *Nat. Rev. Drug Discov.* **1,** 515–528 (2002).
4. Wienken, C. J., Baaske, P., Rothbauer, U., Braun, D. & Duhr, S. Protein-binding assays in biological liquids using microscale thermophoresis. *Nat. Commun.* **1,** 100 (2010).
5. Lin, B., Qiu, et al. A label-free optical technique for detecting small molecule interactions. *Biosens. Bioelectron.* **17,** 827–834 (2002).
6. Olaru, A., Bala, C., Jaffrezic-Renault, N. & Aboul-Enein, H. Y. Surface plasmon resonance (SPR) biosensors in pharmaceutical analysis. *Crit. Rev. Anal. Chem.* **45,** 97–105 (2015).
7. Schuck, P. Use of surface plasmon resonance to probe the equilibrium and dynamic aspects of interactions between biological macromolecules. *Annu. Rev. Biophys. Biomol. Struct.* **26,** 541–566 (1997).
8. Zhao, H., Gorshkova, I. I., Fu, G. L. & Schuck, P. A comparison of binding surfaces for SPR biosensing using an antibody-antigen system and affinity distribution analysis. *Methods* ***59,*** 328–335 (2013).
9. Grüner, S., et al. Impact of protein and ligand impurities on ITC-derived protein-ligand thermodynamics. *Biochim. Biophys. Acta* **1840,** 2843–2850 (2014).
10. Kitova, E. N., El-Hawiet, A., Schnier, P. D. & Klassen, J. S. Reliable determinations of protein-ligand interactions by direct ESI-MS measurements. Are we there yet? *J. Am. Soc. Mass. Spectrom.* **23,** 431–441 (2012).
11. Carpenter, J. F., et al. Potential inaccurate quantitation and sizing of protein aggregates by size exclusion chromatography: Essential need to use orthogonal methods to assure the quality of therapeutic protein products *J. Pharm. Sci.* **99,** 2200–2208 (2010).
12. Clark, S. M. & Konermann, L. Determination of ligand-protein dissociation constants by electrospray mass spectrometry-based diffusion measurements. *Anal. Chem.* **76,** 7077–7083 (2004).
13. Jensen, H. & Østergaard, J. Flow induced dispersion analysis quantifies noncovalent interactions in nanoliter samples. *J. Am. Chem. Soc.* **132,** 4070–4071 (2010).

14. Bielejewska, A., Bylina, A., Duszczyk, K., Fiałkowski, M. & Hołyst, R. Evaluation of ligand-selector interaction from effective diffusion coefficient. *Anal. Chem.* **82,** 5463−6469 (2010).

15. Wätzig, H., et al. Data quality in drug discovery: the role of analytical performance in ligand binding assays. *J. Comput.-Aided Mol. Des.* **29,** 847−865 (2015).

16. Kanoatov, M. et al. Using nonequilibrium capillary electrophoresis of equilibrium mixtures (NECEEM) for simultaneous determination of concentration and equilibrium constant. *Anal. Chem.* **87,** 3099−3106 (2015).

17. Griffiths, A. On the Movement of a Coloured Index along a Capillary Tube, and its Application to the Measurement of the Circulation of Water in a Closed Circuit. *Proc. Phys. Soc. London* **23,** 190−197 (1910).

18. Taylor, G. T. F. R. S. Dispersion of soluble matter in solvent flowing slowly through a tube. *Proc. R. Soc. A: Math. Phys. Eng. Sci.* **219,** 186−203 (1953).

19. Trumbore, C. N., Grehlinger, M., Stowe, M. & Keleher, F. M. Further experiments on a new, fast method for determining molecular weights of diffusing species in a liquid. *J. Chromatogr. A* **322,** 443−454 (1985).

20. Fischer, Ch.-H. & Giersig, M. Analysis of colloids: VII. Wide-bore hydrodynamic chromatography, a simple method for the determination of particle size in the nanometer size regime. *J. Chromatogr. A* **688,** 97−105 (1994).

21. Umehara, R., Miyahara, H., Okino, A., Harada, M. & Okada, T. Wide-bore capillary hydrodynamic chromatography with ICP-MS detection for evaluation of lanthanide uptake by molecular aggregates. *Anal. Sci.* **28,** 359−365 (2012).

22. Chamieh, J., et al. Limits in size of Taylor dispersion analysis: representation of the different hydrodynamic regimes and application to the size-characterization of cubosomes. *Anal. Chem.* **89,** 13487−13493 (2017).

23. Umehara, R., Harada, M. & Okada, T. Wide-bore hydrodynamic chromatography in sub-second range. *J. Sep. Sci.* **32,** 472−478 (2009).

24. di Cagno, M. P., et al. Experimental Determination of Drug Diffusion Coefficients in Unstirred Aqueous Environments by Temporally Resolved Concentration Measurements. *Mol. Pharmaceutics* **15,** 1488−1494 (2018).

25. Okhonin, V., Wong, E. & Krylov, S.N. Mathematical model for mixing reactants in a capillary microreactor by transverse diffusion of laminar flow profiles. *Anal. Chem.* **80,** 7482−7486 (2008).

26. Harada, M., Kido, T., Masudo, T. & Okada, T. Solute distribution coupled with laminar flow in wide-bore capillaries: What can be separated without chemical or physical fields? *Anal. Sci.* **21,** 491−496 (2005).

27. Okada, T., Harada, M. & Kido, T. Resolution of small molecules by passage through an open capillary. *Anal. Chem.* **77,** 6041−6046 (2005).

28. Schramke, J. A., Murphy, S. F., Doucette, W. J. & Hintze, W. D. Prediction of aqueous diffusion coefficients for organic compounds at 25 °C. *Chemosphere* **38,** 2381-2406 (1999).

29. Sowole, M.A., Vuong, S. & Konermann, L. Interactions of hemoglobin and myoglobin with their ligands CN^-, CO, and O_2 monitored by electrospray ionization-mass spectrometry. *Anal. Chem.* **87,** 9538−9545 (2015).

30. Molki, A., Khezzar, L. & Goharzadeh, A. Measurement of fluid velocity development in laminar pipe flow using laser Doppler velocimetry. *Eur. J. Phys.* **34,** 1127−1134 (2013).

31. Andersson, L.-O., Rehnstrom, A. & Eaker, D.L. Studies on "nonspecific" binding. The nature of the binding of fluorescein to bovine serum albumin. *Eur. J. Biochem.* **20,** 371−380 (1971).

32. Pinger, C. W., Castiaux, A., Speed, S. & Spence, D. M. Plate reader compatible 3D-printed device for teaching equilibrium dialysis binding assays. *J. Chem. Educ.* **95,** 1662−1667 (2018).

33. Munson, M. S., Meacham, J. M., Locascio, L. E. & Ross D. Counterflow rejection of adsorbing proteins for characterization of biomolecular interactions by temperature gradient focusing. *Anal. Chem.* **80,** 172−178 (2008).

34. Imamura, H., Komori, T., Ismail, A., Suenaga, A. & Otagiri, M. Stereoselective protein binding of alprenolol in the renal diseased state. *Chirality* **14,** 599−603 (2002).

35. Bao, J. et al. Kinetic capillary electrophoresis with mass-spectrometry detection (KCE-MS) facilitates label-free solution-based kinetic analysis of protein-small molecule binding. *ChemBioChem* **12,** 2551−2554 (2011).

36. McDonnel, P. A., Caldwell, G. W. & Masucci, J. A. Using capillary electrophoresis/frontal analysis to screen drugs interacting with human serum proteins. *Electrophoresis* **19,** 448−454 (1998).

37. Yasgar, A., et al. High-throughput 1,536-well fluorescence polarization assays for α1-acid glycoprotein and human serum albumin binding. *PLoS One* **7,** e45594 (2012).